Microfluidics and Nanofluidics (2019) 23:89
https://doi.org/10.1007/s10404-019-2253-7

RESEARCH PAPER

Numerical simulations of the motion of ellipsoids in planar Couette flow of Giesekus viscoelastic fluids

Yelong Wang[1] · Zhaosheng Yu[1] · Jianzhong Lin[1]

Received: 31 January 2019 / Accepted: 18 May 2019 / Published online: 11 June 2019

Abstract
The motion of neutrally buoyant ellipsoids in a planar Couette flow of Giesekus viscoelastic fluids between two narrowly set plates is numerically simulated with a fictitious domain method. The aspect ratio of the ellipsoid is 4 (i.e., prolate spheroids) and the Deborah number (*De*) ranges from 0 to 4.0. For a single ellipsoid initially placed in the mid-plane between the two plates, the ellipsoid major axis rotates around the vorticity axis in a kayaking mode at relatively low Deborah numbers, and is tilted in the flow-vorticity plane when the Deborah number exceeds a critical value, with the orientation being closer to the flow direction for a larger *De*. For a single ellipsoid initially not placed in the mid-plane, the ellipsoid undergoes lateral migration toward the nearby wall, and it is interesting that the ellipsoid turns its orientation to the vorticity axis at relatively small *De* and a direction close to the vorticity axis at large *De* (above 3.0), in contrast to the ellipsoid placed in the mid-plane without lateral migration, whose terminal orientation exhibits a kayaking motion at relatively small *De* and is close to the flow direction for $De > 3$. As a result, for the multiple-ellipsoid case, there exists a transient stage where the average orientation of the ellipsoids turns toward the vorticity axis for all nonzero Deborah numbers studied, and the orientation close to the vorticity axis can be often observed for the isolated ellipsoids. Both the particle interactions and the wall effect promote the ellipsoids to align with the flow direction. Particle aggregation and the dynamic aligning structures are observed at large Deborah numbers.

Keywords Lateral migration · Planar Couette flow · Giesekus viscoelastic fluid · Ellipsoid

1 Introduction

The motion of particles in a fluid is a topic of extensive studies. In many applications particles are non-spherical, like ellipsoids or cylinders. The motion of a non-spherical particle in fluids is complicated because the particle rotation or orientation is strongly coupled with its translational motion due to the shape anisotropy. The dynamics becomes even more complex when the suspending fluid is a non-Newtonian fluid. The orientation distribution of non-spherical particles influences significantly the final properties of the product. Understanding the dynamics of the orientation distribution of non-spherical particles suspended in non-Newtonian fluids is important to the production process optimization and the novel technology development for particle manipulation.

For the motion of an ellipsoidal particle in a Newtonian fluid, a closed trajectory called the Jeffery orbit (Jeffery 1922) was found for the orientation under the condition of Stokes flow. The orientation of a spheroid in Couette flow at moderately high Reynolds numbers was studied by various groups (e.g., Qi and Luo 2003; Yu et al. 2007; Huang et al. 2012; Rosén et al. 2015), and it was observed that the orientation of the spheroid experienced the transitions, as the Reynolds number was increased. The motion of a single neutrally suspending ellipsoid in a three-dimensional pipe was studied by Karnis et al. (1966), Pan et al. (2008) and Huang and Lu (2017).

The dynamics of non-spherical particles in non-Newtonian fluids has attracted much attention over the past few

This article is part of the topical collection "Particle motion in non-Newtonian microfluidics" guest edited by Xiangchun Xuan and Gaetano D'Avino.

✉ Zhaosheng Yu
yuzhaosheng@zju.edu.cn

✉ Jianzhong Lin
jzlin@zju.edu.cn

[1] State Key Laboratory of Fluid Power and Mechatronic System, Department of Mechanics, Zhejiang University, Hangzhou 310027, China

decades (D'Avino and Maffettone 2015). There were many works on the motion of ellipsoidal particles in the unconfined shear flow without particle side migration (Saffman 1956; Gauthier et al. 1971; Bartram et al. 1975). It was found that the rotation of ellipsoids was slower than that in Newtonian fluids at moderate to small shear rates, and the rod-like particles drifted to a log-rolling orbit gradually, while the disk-like particles drifted to a tumbling orbit with the axis of revolution lying in the flow-gradient plane and rotating (Bartram et al. 1975; Leal 1975; Harlen and Koch 1993). It was experimentally validated that this conclusion was still valid in simple shear flow of semi-dilute fiber suspension (Iso et al. 1996a) or carbon nanotubes in polymer melt (Hobbie et al. 2003). Brunn (1980) used the second-order fluid model to analyze the migration of dumbbell and three-dumbbell particles in the simple shear flow field. Cohen et al. (1987) considered the influence of Brownian motion and found that the orientation distribution function for dilute suspensions had bimodal. Particles either remained on Jeffery orbits or ended up in a log-rolling state. A model of short fiber suspensions in second-order fluids was proposed by Borzacchiello et al. (2016). Férec et al. (2017) derived a complete rheological constitutive equation for dilute and semi-dilute slender rod suspensions in a viscoelastic fluid with low elasticity.

For higher shear or elastic effects, the direction of the major axis of the prolate ellipsoid or fibers tended to change from the vorticity direction to the flow direction (Bartram et al. 1975; Iso et al. 1996b). The principal axis of the prolate ellipsoid could stabilize in some directions between the vorticity direction and the flow direction (Johnson et al. 1990). The direction of the major axis of a disk with an aspect ratio of 0.68 was found to keep rotating in different equilibrium orbits at moderate shear rates in Couette flow of 2.5% polyacrylamide in water solution (Bartram et al. 1975). The orientation of a prolate ellipsoidal particle in viscoelastic shear flow field without inertial effect was investigated numerically by D'Avino et al. (2014). They identified four different regimes, depending on the Deborah number: the particle major axis is drifted toward the vorticity axis (i.e., log-rolling) at relatively low *De* (region I); the major axis is tilted in the flow-vorticity plane, with the orientation closer to the flow direction for a higher *De* (region II); both tilted and flow alignment orientations exist at the same *De* (region III with bistability scenario), and only alignment along the flow direction is stable at high *De* (region IV). The rheology of a dilute viscoelastic suspension of spheroids subjected to unconfined shear flow was studied numerically by D'Avino et al. (2015), who adopted two viscoelastic constitutive equations, i.e., the Giesekus and the Phan-Thien–Tanner (PTT) models, to examine the effects of the suspending fluid rheology. Their results indicated that for a spheroid suspended in the PTT fluid for the Deborah number ranging from 0 to 4, only first two regimes were identified, i.e., the log-rolling motion (region I), and the tilted orientation (region II). The flow-induced orientation of spheroidal particles in viscoelastic fluids covering a wide range of rotational Peclet and Weissenberg numbers was experimentally studied by Gunes et al. (2008), and the particles were observed to be spinning in Jeffery orbits, a 'log-rolling' state, reorienting in the flow direction, as the shear rate increased.

Numerous works have been devoted to the particle dynamics in the viscoelastic flows with wall confinement (D'Avino et al. 2017; Lu et al. 2017). The lateral motion of a circular particle in viscoelastic Couette and Poiseuille flows was studied by Huang et al. (1997), and it was found that the shear-thinning enhanced the migration toward the wall. The motion of a particle in the Giesekus viscoelastic Couette flow was simulated in two-dimensional and three-dimensional cases, respectively, and the particle lateral migration toward the wall was revealed (D'Avino et al. 2010a, b), which was later confirmed experimentally (Caserta et al. 2010). The effects of particle surface slip and wall slip on the dynamics of a spherical particle in Newtonian and viscoelastic fluids subjected to shear and Poiseuille flows were studied by Trofa et al. (2016a, b). The lateral migration of a neutrally buoyant spherical particle in a pressure-driven rectangular-shaped channel flow of Giesekus viscoelastic fluids was numerically investigated by Wang et al. (2018). Lin et al. (2018) examined the effects of Stokes number, Weissenberg number, particle aspect ratio and particle-to-fluid density ratio on the mixing and orientation distributions of cylindrical particles in a mixing layer of an Oldroyd-B fluid. A fractionation technique for non-Brownian rod-like particle suspensions based on the control of the threshold for motion in a yield stress fluid was explored by Madani et al. (2010). D'Avino et al. (2019) investigated the dynamics of a spheroidal particle with an aspect ratio of 2 suspended in a viscoelastic, shear-thinning liquid flowing in a wide-slit pressure-driven micro-channel at low and moderate Weissenberg numbers, and observed that the particle always tended to align along the flow direction while migrating toward the center-plane of the channel.

The chaining of particles in non-Newtonian oscillating shear flow was early studied by Michele et al. (1977). The formed 'chains' were found to be longer, as the number of inversion cycles of the plates and the shear rate increased. The chaining of particles in shear-thinning viscoelastic fluids was studied by Won and Kim (2004) and Scirocco et al. (2004). The shear-thinning was regarded as a condition for particle aggregation. No alignment was observed in highly elastic Boger fluids without shear-thinning effect (Scirocco et al. 2004). Necklaces of particles aligned in the flow direction were observed, while the role of particle migration was found to be important (Pasquino et al. 2010). The degree of alignment increased with increasing

shear rate and particle size and with decreasing gap. Particles migrated toward the plates, where the particles assembled and aligned in strings in the flow direction. For the small particles, the formation of particle doublets or short strings along the vorticity direction was observed at low shear rates, which flipped to the flow direction and grew into longer strings at higher shear rates (Pasquino et al. 2010). Pasquino et al. (2013) investigated experimentally the microstructure formation of dilute sphere suspensions in a viscoelastic fluid by optical microscopy techniques at volume fractions ranging between 0.1 and 1.0%, and the results showed that the particle strings grew faster and longer, as the shear rate or the particle volume fraction increased. The migration and chaining of non-colloidal spheres in a worm-like micellar, viscoelastic solution in shear flow were studied experimentally and by 2D numerical simulations (Pasquino et al. 2014). Their experimental results showed the formation of particle chains in the bulk region, along with migration of a considerable fraction of spheres to the walls. Numerical simulations with the Giesekus viscoelastic constitutive equation reproduced the same phenomena observed experimentally, both in terms of fast particle migration to the wall and bulk chain stability. No alignment was found in simulations with a constant-viscosity, elastic fluid (Oldroyd-B model), in agreement with previous experimental results with Boger fluids of Scirocco et al. (2004). Alignment and segregation of bidisperse colloids in a shear-thinning viscoelastic fluid under shear flow was numerically investigated by de Oliveira et al. (2013). When the distance between the plates was much larger than the of the particle diameter, the large and small particles were chained separately, unlike a narrow plate system, where the large and small particles were chained together (Lyon et al. 2001). Jaensson et al. (2016) presented for the first time 3D direct numerical simulations of the alignment of two and three rigid, non-Brownian spherical particles in a viscoelastic shear flow, and showed that alignment was mainly governed by the value of the elasticity parameter S, defined as half of the ratio between the first normal stress difference and shear stress of the suspending fluid. The experimental results of Gunes et al. (2008) indicated that it was more difficult for the prolate spheroids to form aggregates in the shear flow of viscoelastic fluids, compared to the spherical particles.

In the present study, the motion of spheroids in a Couette flow of Giesekus viscoelastic fluids at low Reynolds numbers is examined with direct numerical simulations. In Sect. 2, the fictitious domain method used, the collision model and the simulation set-up are described. In Sect. 3, the results on a single spheroid with its center fixed in the mid-plane without migration, a single spheroid released at an off-center position with migration, and the multiple-particles are reported and discussed. The concluding remarks are given in the final section.

2 Numerical model

2.1 Fictitious domain method

The direct-forcing fictitious domain (DF/FD) method (Yu and Shao 2007) is employed to simulate the motion of ellipsoids in Couette flow. This method is an improved version of the earlier distributed-Lagrange-multiplier/fictitious domain (DLM/FD) code (Yu et al. 2002, 2006; Yu and Wachs 2007) which was originally developed by Glowinski et al. (1999). We only briefly describe the method used in the following, and the reader is referred to Yu and Shao (2007) for further details of the method. Let Ω the entire domain including interior and exterior of the solid body and $P(t)$ represent the solid domain. The fluid density is ρ_f. The ellipsoidal particle density, volume, moment of inertia, translational velocity, and angular velocity are ρ_s, V_p, $\mathbf{J}$, $\mathbf{U}$ and $\boldsymbol{\omega}_s$, respectively. Suppose that the fluid solvent viscosity and polymer viscosity are η_s and η_p, respectively. By introducing the following scales for the nondimensionalization: H for length, U_c for velocity, H/U_c for time, $\rho_f U_c^2$ for the pressure, and $\rho_f U_c^2/H$ for the pseudo body force, the dimensionless FD formulation for an incompressible Giesekus viscoelastic fluid suspended with neutrally buoyant ellipsoids comprises the following three parts:

a. Continuity equation

$$\nabla \cdot \mathbf{u} = 0 \quad \text{in } \Omega \tag{1}$$

b. Combined momentum equations

$$\frac{\partial \mathbf{u}}{\partial t} + \mathbf{u} \cdot \nabla \mathbf{u} = -\nabla p + \eta_r \frac{\nabla^2 \mathbf{u}}{Re} + \frac{(1-\eta_r)\nabla \cdot \mathbf{B}}{ReDe} + \mathbf{f} \quad \text{in } \Omega \tag{2}$$

$$\mathbf{u} = \mathbf{U} + \boldsymbol{\omega}_s \times \mathbf{r} \quad \text{in } P(t) \tag{3}$$

$$(\rho_r - 1) V_p^* \frac{\mathrm{d}\mathbf{U}}{\mathrm{d}t} = -\int_P \mathbf{f}\,\mathrm{d}\mathbf{x} \tag{4}$$

$$(\rho_r - 1) \frac{\mathrm{d}(\mathbf{J}^* \cdot \boldsymbol{\omega}_s)}{\mathrm{d}t} = -\int_P \mathbf{r} \times \mathbf{f}\,\mathrm{d}\mathbf{x} \tag{5}$$

c. Giesekus constitutive equation

$$\frac{\partial \mathbf{B}}{\partial t} + \mathbf{u} \cdot \nabla \mathbf{B} - (\nabla \mathbf{u})^T \cdot \mathbf{B} - \mathbf{B} \cdot \nabla \mathbf{u} + \frac{\alpha}{De}(\mathbf{B} - \mathbf{I})^2 + \frac{\mathbf{B} - \mathbf{I}}{De} = 0 \quad \text{in } \Omega \tag{6}$$

In the above equations, $\mathbf{u}$ represents the fluid velocity, p the fluid pressure, $\mathbf{f}$ the Lagrange multiplier that is defined in the solid domain $P(t)$, $\mathbf{r}$ the position vector with respect to the mass center of the particle, ρ_r the particle–fluid density ratio defined by $\rho_r = \rho_s/\rho_f$, Re the Reynolds number defined by $Re = \rho_f U_c H/\eta_0$ (η_0 being the total zero shear-rate viscosity of the fluid $\eta_0 = \eta_s + \eta_p$), V_p^* the dimensionless particle volume define by $V_p^* = V_p/H^3$, $\mathbf{J}^*$ the dimensionless moment of inertia defined by $\mathbf{J}^* = \mathbf{J}/\rho_s H^5$, $\eta_r = \eta_s/\eta_0$, De the Deborah number defined as $De = \lambda U_c/H$ (λ being the fluid relaxation time), $\mathbf{B}$ the polymer configuration tensor which is related to the polymer stress tensor $\boldsymbol{\tau}$ via $\boldsymbol{\tau} = \eta_p(\mathbf{B}-\mathbf{I})/\lambda$ and α a parameter in the Giesekus model, which reduces to the Oldroyd-B model for $\alpha = 0$.

A fractional-step time scheme is used to decouple systems (1)–(6) into the following three sub-problems.

a. Fluid sub-problem for $\mathbf{u}^*$ and p

$$\frac{\mathbf{u}^* - \mathbf{u}^n}{\Delta t} - \eta_r \frac{\nabla^2 \mathbf{u}^*}{2Re} = -\nabla p + \frac{1}{2}(3\mathbf{G}^n - \mathbf{G}^{n-1}) + \eta_r \frac{\nabla^2 \mathbf{u}^n}{2Re} + \mathbf{f}^n \tag{7}$$

$$\nabla \cdot \mathbf{u}^* = 0 \tag{8}$$

where $\mathbf{G} = -\mathbf{u}\cdot\nabla\mathbf{u} + [(1-\eta_r)/ReDe]\nabla\cdot\mathbf{B}$. This sub-problem is essentially the solution of the Navier–Stokes equation. An efficient finite-difference-based projection method on a homogeneous half-staggered grid is employed (Yu and Shao 2007). All spatial derivatives are discretized with the second-order central difference scheme.

b. Particle sub-problem for $\mathbf{U}^{n+1}$, $\boldsymbol{\omega}_s^{n+1}$

$$\rho_r V_p^* \frac{\mathbf{U}^{n+1}}{\Delta t} = (\rho_r - 1) V_p^* \frac{\mathbf{U}^n}{\Delta t} + \int_P \left(\frac{\mathbf{u}^*}{\Delta t} - \mathbf{f}^n\right) \mathrm{d}\mathbf{x} \tag{9}$$

$$\rho_r \frac{\mathbf{J}^* \cdot \boldsymbol{\omega}_s^{n+1}}{\Delta t} = (\rho_r - 1)\left[\frac{\mathbf{J}^* \cdot \boldsymbol{\omega}_s^n}{\Delta t} - \boldsymbol{\omega}_s^n \times (\mathbf{J}^* \cdot \boldsymbol{\omega}_s^n)\right] + \int_p \mathbf{r} \times \left(\frac{\mathbf{u}^*}{\Delta t} - \mathbf{f}^n\right) \mathrm{d}\mathbf{x} \tag{10}$$

Note that the above equations have been reformulated so that all the right-hand side terms are known quantities and consequently the particle velocities $\mathbf{U}^{n+1}$, $\boldsymbol{\omega}_s^{n+1}$ are obtained without iteration. Then, the Lagrange multipliers defined at the Lagrangian nodes are determined from:

$$\mathbf{f}^{n+1} = \frac{\mathbf{U}^{n+1} + \boldsymbol{\omega}_s^{n+1} \times \mathbf{r} - \mathbf{u}^*}{\Delta t} + \mathbf{f}^n \tag{11}$$

Finally, the fluid velocities $\mathbf{u}^{n+1}$ at the Eulerian nodes are corrected from

$$\mathbf{u}^{n+1} = \mathbf{u}^* + \Delta t\left(\mathbf{f}^{n+1} - \mathbf{f}^n\right) \tag{12}$$

In the above manipulations, the tri-linear function is used to transfer the fluid velocity from the Eulerian nodes to the Lagrangian nodes, and distribute the pseudo body force from the Lagrangian nodes to the Eulerian nodes.

The orientation of the ellipsoids is calculated using the quaternions. Quaternions are real numbers (q_1, q_2, q_3, q_4). The time-evolution of the quaternions is related to the angular velocity $\boldsymbol{\omega}_s$:

$$\begin{pmatrix} \dot{q}_1 \\ \dot{q}_2 \\ \dot{q}_3 \\ \dot{q}_4 \end{pmatrix} = \frac{1}{2}\begin{pmatrix} q_4 & -q_3 & -q_2 & q_1 \\ q_3 & q_4 & -q_1 & q_2 \\ -q_2 & q_1 & q_4 & q_3 \\ -q_1 & -q_2 & -q_3 & q_4 \end{pmatrix}\begin{pmatrix} \omega_{sx} \\ \omega_{sy} \\ \omega_{sz} \\ 0 \end{pmatrix} \tag{13}$$

The transform matrix A from the ellipsoid's body coordinate frame to the space-fixed coordinate frame is:

$$A = 2\begin{pmatrix} q_1^2 + q_4^2 - 1/2 & q_1q_2 + q_3q_4 & q_1q_3 - q_2q_4 \\ q_1q_2 - q_3q_4 & q_2^2 + q_4^2 - 1/2 & q_2q_3 + q_1q_4 \\ q_1q_3 + q_2q_4 & q_2q_3 - q_1q_4 & q_3^2 + q_4^2 - 1/2 \end{pmatrix} \tag{14}$$

c. Constitutive equation sub-problem for $\mathbf{B}$

$$\frac{\mathbf{B}^{n+1} - \mathbf{B}^n}{\Delta t} + \mathbf{u}^{n+1}\cdot\nabla\mathbf{B}^n - \left(\nabla\mathbf{u}^{n+1}\right)^T \cdot \mathbf{B}^n - \mathbf{B}^n \cdot \nabla\mathbf{u}^{n+1} + \frac{\alpha}{De}(\mathbf{B}^n - \mathbf{I})^2 + \frac{\mathbf{B}^{n+1} - \mathbf{I}}{De} = 0 \tag{15}$$

$\mathbf{u}^{n+1}$ in the above equation has been obtained from the fluid sub-problem. For simplicity, only the first-order time scheme is used for the constitutive equation. For the spatial schemes, the convective term is discretized with a third-order upwinding MUSCL scheme (Leer 1979) and the velocity gradient is discretized with the central difference scheme.

2.2 Collision strategy

A particle–particle collision model is required to prevent the mutual penetration of particles. A discrete element model (DEM) is used to deal with collision. Our collision model for the spheroids is obtained from the modification of DEM for the spherical particle. In the following, we first describe the collision model for the spheres. The basic idea of DEM is to simulate the interactions between particles using springs, viscous pots and other elements, taking into account the normal and tangential effects between particles (Crowe et al. 2011). For spherical particles, the normal and tangential forces are as follows:

$$\mathbf{F}_n = \left(-k_n\delta_n^{3/2} - \eta_n\mathbf{G}\cdot\mathbf{n}\right)\mathbf{n} \tag{16}$$

$$\mathbf{F}_t = -k_t\boldsymbol{\delta}_t - \eta_t\mathbf{G}_{ct} \tag{17}$$

$\mathbf{n}$ is the unit normal vector of the action. $\mathbf{F}_n$, δ_n, k_n, η_n are the normal force acting on particle 1, the normal overlap distance, the normal spring coefficient and the normal viscous pot coefficient are, respectively applied, where $\mathbf{F}_t$, δ_t, k_t, η_t are the corresponding tangent vectors. $\mathbf{G}$ is the relative velocity of two particle centers of mass; vector $\mathbf{G}_{\mathrm{ct}}$ is the slip velocity, which is defined as follows:

$$\mathbf{G}_{\mathrm{ct}} = \mathbf{G} - (\mathbf{G}\cdot\mathbf{n})\mathbf{n} + r_1\boldsymbol{\omega}_{s1}\times\mathbf{n} + r_2\boldsymbol{\omega}_{s2}\times\mathbf{n} \tag{18}$$

r_1, r_2 represent the radii of two particle, and $\boldsymbol{\omega}_{s1}$ and $\boldsymbol{\omega}_{s2}$ are angular velocities of two particle. The normal and tangential forces are assumed to satisfy the friction theorem. The friction coefficient is 0.3 for the collision between particles and 0.2 between particles and walls, respectively. The spring coefficient is given by Hertzian contact theory:

$$k_n = \frac{4}{3}\left(\frac{1-\sigma_i^2}{E_i} + \frac{1-\sigma_j^2}{E_j}\right)^{-1}\left(\frac{r_1+r_2}{r_1r_2}\right)^{-1/2} \tag{19}$$

where E is Young's modulus and σ is the Poisson ratio. The coefficients k_t is given by Mindlin's theory:

$$k_t = 8\left(\frac{2-\sigma_i}{G_i} + \frac{2-\sigma_j}{G_j}\right)^{-1}\left(\frac{r_1+r_2}{r_1r_2}\right)^{-1/2}\delta_n^{1/2} \tag{20}$$

where G is the shear modulus of particles, which is related to Young's modulus and Poisson's ratio of particles: $G = \frac{E}{2(1+\sigma)}$. In the above equations, $\eta_n = 2\sqrt{Mk_n}\quad \eta_t = 2\sqrt{Mk_t}$. M is the mass of the particles.

For ellipsoids, we assume that collision is activated when the distance between the surfaces of two spheroids is smaller than a critical value $d_c = h$, where h is the mesh spacing used. We adopt an efficient iterative method proposed by Lin and Han (2002) to determine the positions of two points of shortest distance between two spheroids and then take the connector of these two points as the normal direction. The radii of spherical particles in the corresponding formula are replaced by the equivalent radius r_e of ellipsoidal particles. The equivalent radius of an ellipsoidal particle is taken as the average of the radii of the three principal axes of an ellipsoid. Young's modulus and Poisson's ratio are taken as $E = 3\times10^4$ and $\sigma = 0.33$. The time step of discrete element model is $\Delta t/10$, where Δt is the time step for the solution of the flow.

The purpose of the collision model is to prevent the particle mutual penetration. DEM allows slight penetration between particles, but this does not cause any problem both physically (slight penetration means particle deformation) and numerically for our FD method. The particle motion is mainly dominated by the hydrodynamic force, rather than the collision.

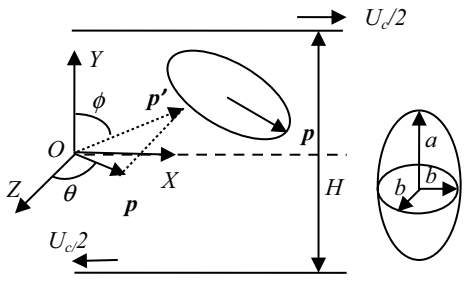

Fig. 1 Schematic diagram of a prolate ellipsoid suspended in planar Couette flow

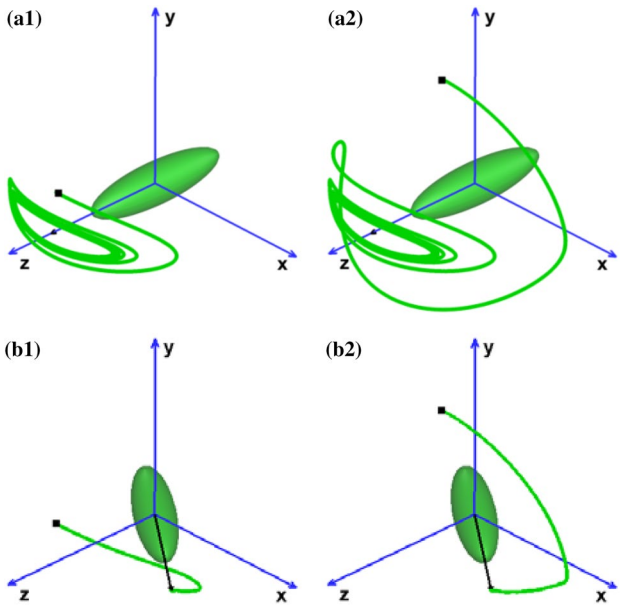

Fig. 2 Orbits described by the orientation vector for the ellipsoid (green line) for $De = 1.0$ (**a1**, **a2**), $De = 2.7$ (**b1**, **b2**). The initial orientation vector for the left two panels is (0, 0.31, 0.95), while the initial orientation vector for the right two panels is (0, 0.95, 0.31). The black vector represents the terminal orientation vector for the ellipsoid (color figure online)

2.3 Simulation setup

The physical model studied is shown in Fig. 1. The upper and lower walls are flat plates with opposite velocity $U_c/2$. The distance between two plates is H. The computational domain is a cubic cell $[0, H]\times[-H/2, H/2]\times[0, H]$. The periodic boundary conditions are imposed in the directions of flow (x) and vorticity (z). The semi-major axis of the ellipsoid is $a = H/6$, the semi-minor axis is $b = H/24$, and the aspect ratio is $A_r = a/b = 4$. We take U_c and H as the characteristic velocity and length, respectively, thus the time is scaled as the inverse of the shear rate.

The ratio of the length of ellipsoid major axis to the distance between the two plates is defined as the blockage

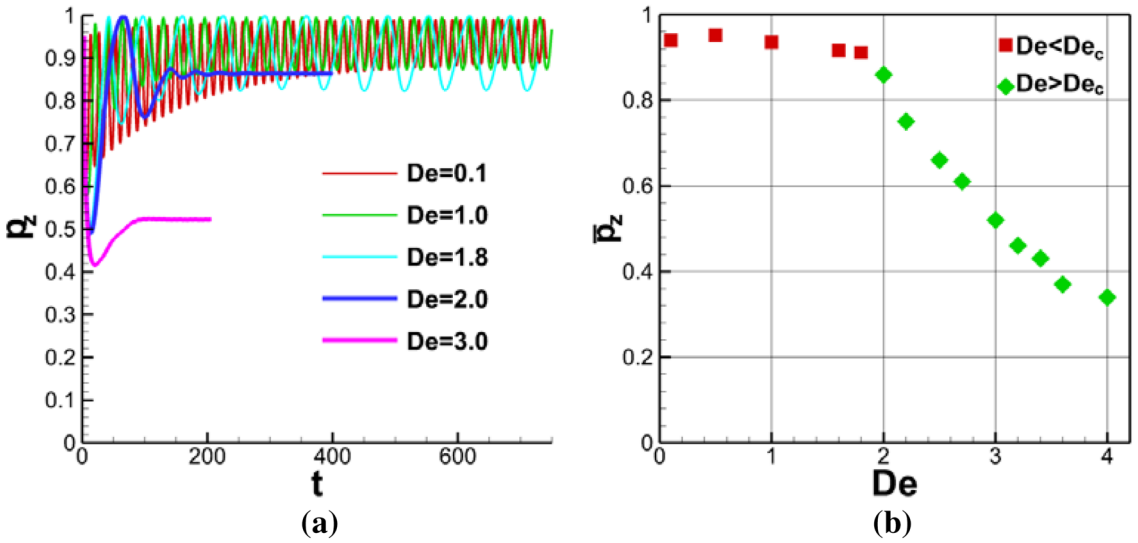

Fig. 3 **a** The value of z-component of the orientation vector as a function of time for different Deborah numbers, and **b** the average value of z-component of the orientation vector as a function of Deborah number at stable or steady state

ratio, $\beta = 2a/H = 1/3$. The number of the ellipsoids in the cubic cell is denoted by N_p. The Reynolds number based on U_c and H is set to be $Re = 0.5$, as an approximation to the Stokes flow. Note that the particle Reynolds number measuring the fluid inertial effect on the particle in a shear flow is $Re_p = \rho_f(2a)^2\dot{\gamma}/\eta_0 = Re(2a/H)^2 \approx 0.055$. It was shown that a prolate followed the Jeffery orbit well at $Re_p = 0.5$ (Yu et al. 2007). Therefore, the fluid inertial effect is expected to be negligibly small for $Re = 0.5$. The mesh size is $h = H/128$, and the time step is $\Delta t = 5 \times 10^{-4}$. The computational cost is high due to millions of time steps required, and it typically took several months CPU time to run a case. For the Giesekus model used, the parameters are $\alpha = 0.2$, and $\eta_r = 0.091$, following D'Avino et al. (2014).

3 Results and discussion

The motion of neutrally suspended ellipsoids with the aspect ratio $A_r = 4$ in planar Couette flow of Giesekus viscoelastic fluid is simulated for $N_p = 1$, 18, 54 respectively. In the following, (x_p, y_p, z_p) is used to represent the coordinates of an ellipsoid center, and (p_x, p_y, p_z) is used to represent the ellipsoid orientation vector .

3.1 Motion of a single ellipsoid

a. Initially placed in the mid-plane between the two plates

The motion of a single ellipsoid initially placed in the mid-plane between the two plates is first simulated. Due to the geometric symmetry and the zero velocity of the flow field in the mid-plane, the position of the ellipsoid remains unchanged.

For the Newtonian fluid at $De = 0$, the ellipsoid rotates continuously in the shear flow along the Jeffery orbit (Jeffery 1922). At $De = 1$, the orientation of the ellipsoid first drifts toward the vorticity direction, but it will not reach the log-rolling mode, instead, its stable mode is a kayaking motion, as shown in Fig. 2a. As De is increased beyond a critical value De_c ($1.8 < De_c < 2$), the ellipsoid turns its

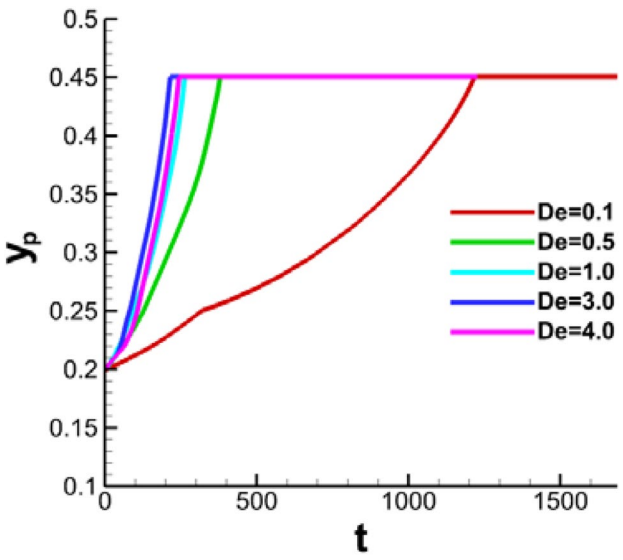

Fig. 4 Evolutions of dimensionless lateral positions of an ellipsoid suspended in Couette flow of a viscoelastic fluid for different Deborah numbers. The ellipsoid has an initial orientation of (0, 0.31, 0.95)

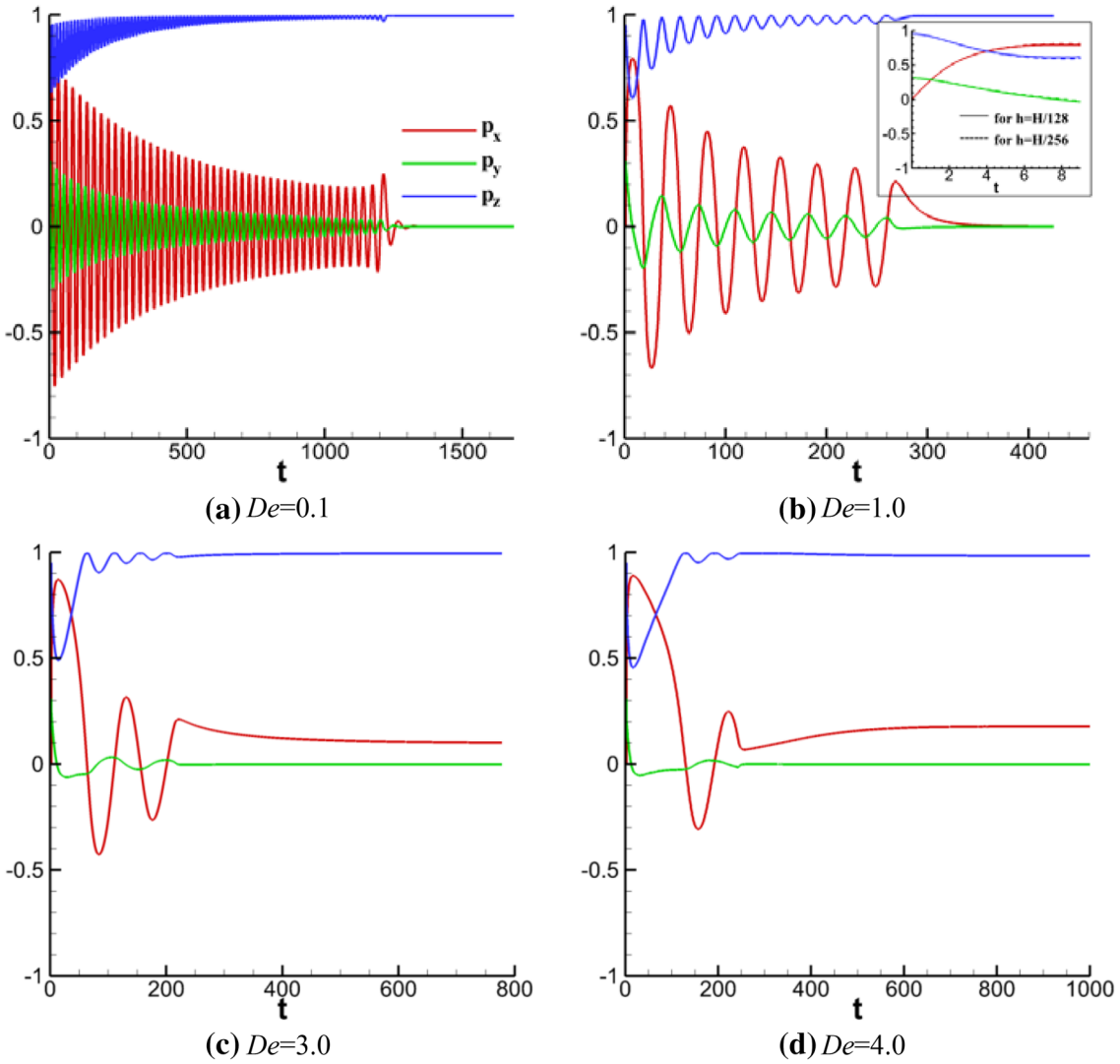

Fig. 5 Time developments of three components of the ellipsoid orientation vector for different Deborah numbers with the same initial orientation vector (0, 0.31, 0.95). **a** $De = 0.1$, **b** $De = 1.0$, **c** $De = 3.0$, **d** $De = 4.0$. The insert in **b** shows the grid-independence test for early time

major axis into the flow-vorticity plane (i.e., x–z plane), and keeps moving in this plane till it reaches a stable orientation. The stable orientation becomes closer to the flow direction, as De increases. The terminal orientation is independent of the initial orientation, as shown in Fig. 2. Figure 3a shows the evolutions of the z-component of the orientation vector for different Deborah numbers, demonstrating the periodic kayaking motion for $De \leq 1.8$, and the stable orientation for $De \geq 2.0$. The average z-component of the orientation vector as a function of Deborah number at stable or steady state is plotted in Fig. 3b.

D'Avino et al. (2014) computed the orientation of a prolate ellipsoidal particle in unbounded shear flow of Giesekus fluids without inertial effect. They identified four different modes, depending on the Deborah number: log-rolling mode (region I); tilted orientation in the flow-vorticity plane, with the orientation closer to the flow direction for a higher De (region II); co-existence of tilted and flow alignment orientations (region III with bistability scenario), and only alignment along the flow direction (region IV). Instead of the log-rolling mode, our results show the kayaking mode around the vorticity axis for relatively low Deborah numbers. The regimes of the bistability and the alignment in the flow direction in D'Avino et al. (2014) are also not observed in our simulations. Our critical Deborah number for the transition between the kayaking and tilted orientations is close to that of D'Avino et al. (2014) for the transition between the log-rolling and tilted orientations (i.e., around 2.0). The main difference in two models lies in the boundary condition: we adopt a relatively narrow Couette system with periodic boundary conditions in the streamwise and spanwise directions, whereas D'Avino et al. (2014) considered a

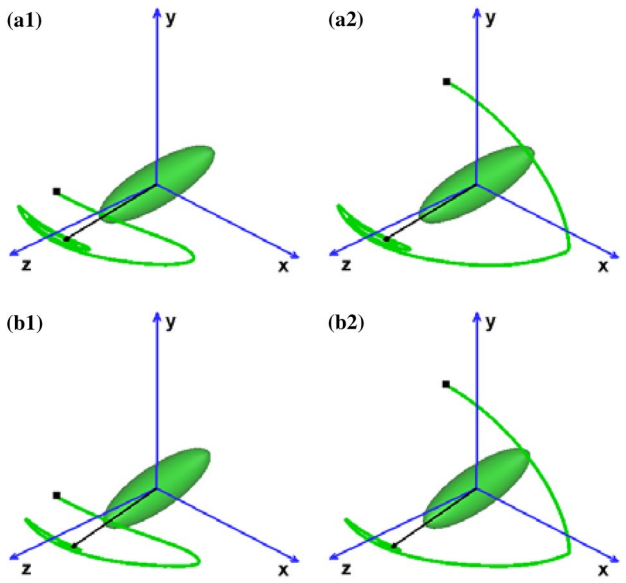

Fig. 6 Orbits described by the orientation vector for the ellipsoid (green line) at $De = 3.0$ (**a1**, **a2**), $De = 4.0$ (**b1**, **b2**). The initial orientation vector for the left two panels is (0, 0.31, 0.95), while the initial orientation vector for the right two panels is (0, 0.95, 0.31). The black vector represents the terminal orientation vector for the ellipsoid (color figure online)

large computational domain with the undisturbed boundary conditions on the outer boundaries, i.e., unbounded shear flow. In addition, $Re = 0$ in D'Avino et al. (2014). It is also possible that the discrepancy is caused by the inaccuracy of our fictitious domain method, since it is a non-boundary-fitted method. The non-boundary-fitted method has the inherent drawback of lower accuracy, but has the advantage of easily dealing with many particles, compared to the boundary-fitted finite element method. The good agreement between two results on the critical Deborah number indicates that the accuracy of our simulations is reasonable and acceptable. Our results below for $De > 3$ are probably not quantitatively accurate, but are expected to be qualitatively reliable, in the sense that the results might correspond to those for the Giesekus fluid at a lower Deborah number or for the PTT fluid.

b. Initially not placed in the mid-plane

The motion of a single ellipsoid initially not placed in the mid-plane between two plates is considered. The initial position of the ellipsoid is (0.5, 0.2, 0.5), and the initial major axis is in the yz plane (the angle with the z-axis is 0.1π or 0.4π). The Deborah number is 0.1, 0.5, 1.0, 3.0, 4.0, respectively. The ellipsoid released not in the mid-plane migrates laterally toward the side wall, as shown in Fig. 4, like a spherical particle (D'Avino et al. 2010b). The lateral migration is slow at $De = 0.1$, and becomes much faster at $De \geq 0.5$. The migration rate is not sensitive to De for $De \geq 1.0$. The time developments of three components of the ellipsoid orientation vector for different Deborah numbers and initial orientation vectors are shown in Fig. 5. The ellipsoid tends to align with the vorticity direction for $De = 0.1$ and 1.0 or a direction near the vorticity direction in the flow-vorticity plane for $De = 3.0$ and 4.0 after its major axis turns into the flow-vorticity plane. The stable orientation can be achieved after the particle reaches the wall, and is shown to be independent of the initial orientation in Fig. 6 for $De = 3.0$ and 4.0. It is surprising that the lateral migration (i.e., the lateral position) has significant effects on the particle orientation. First, the kayaking mode for the prolate

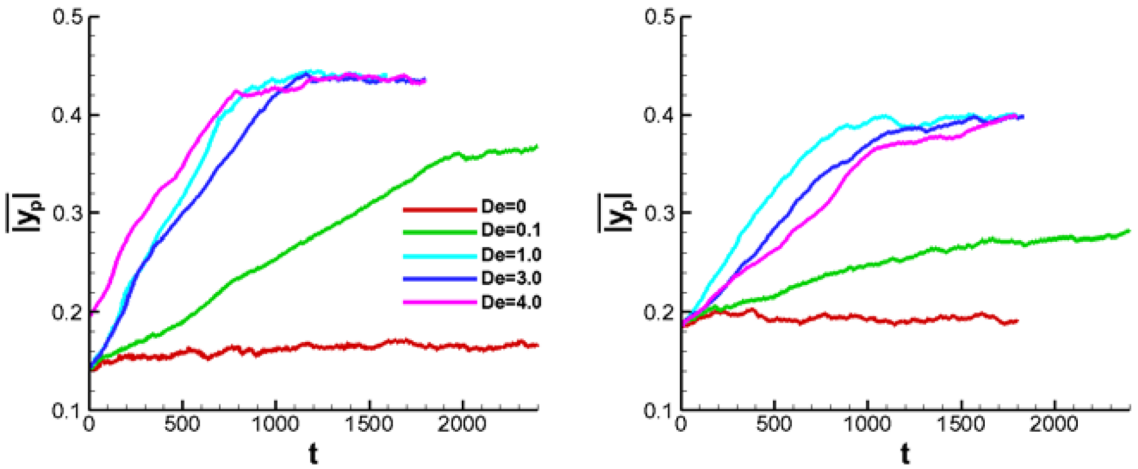

Fig. 7 The time developments of the average dimensionless lateral positions of all ellipsoids with random initial distributions and orientations for different Deborah numbers and two particle numbers, **a** $N_p = 18$, **b** $N_p = 54$

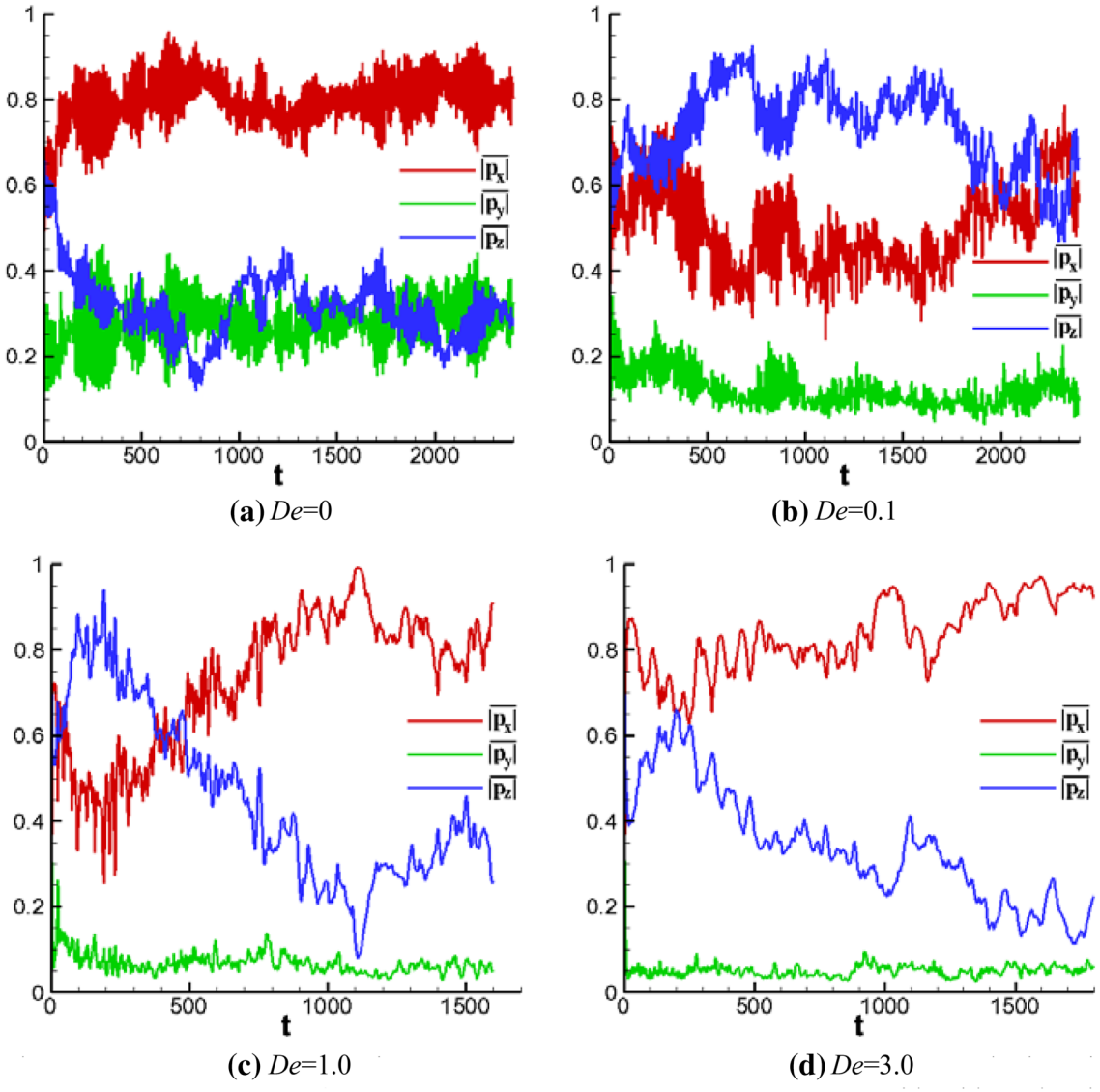

Fig. 8 The time developments of the average orientation components of 18 ellipsoids with random initial distributions and orientations for four Deborah numbers, **a** $De=0$, **b** $De=0.1$, **c** $De=1.0$, **d** $De=3.0$

ellipsoid located in the mid-plane is turned into the log-rolling mode for the ellipsoid near the wall at $De=0.1$ and 1.0. Second, the flow alignment in the mid-plane for $De=3.0$ and 4.0, as shown in Fig. 3 (note that $\cos 45^\circ \approx 0.71$), is turned into the vorticity alignment near the wall. For the present case of a single particle, the wall effect appears to push the particle to align with the vorticity direction. In contrast, for the multiple-particle case, the wall effect tends to lead the particles to align with the flow direction, as shown later. At the moment, we cannot provide a clear explanation for the discrepancy. Further studies are required.

3.2 Motion of multiple ellipsoids

The cases for two particle numbers $N_p=18$ and 54, with corresponding particle volume fractions of 2.18% and 6.54%, respectively, are simulated. Five Deborah numbers $De=0$, 0.1, 1.0, 3.0, 4.0 are considered. $De=0$ represents the Newtonian fluid case. The initial orientations of the ellipsoids are generated randomly with θ in 0–π, and ϕ in 0–2π, where θ and ϕ are shown in Fig. 1. The initial positions of the ellipsoids are also generated randomly without overlap between particles.

For the multiple ellipsoids, we are concerned with the evolutions of their average lateral position $\overline{|y_p|}$ and orientations $\overline{|p_x|}$, $\overline{|p_y|}$, $\overline{|p_z|}$.

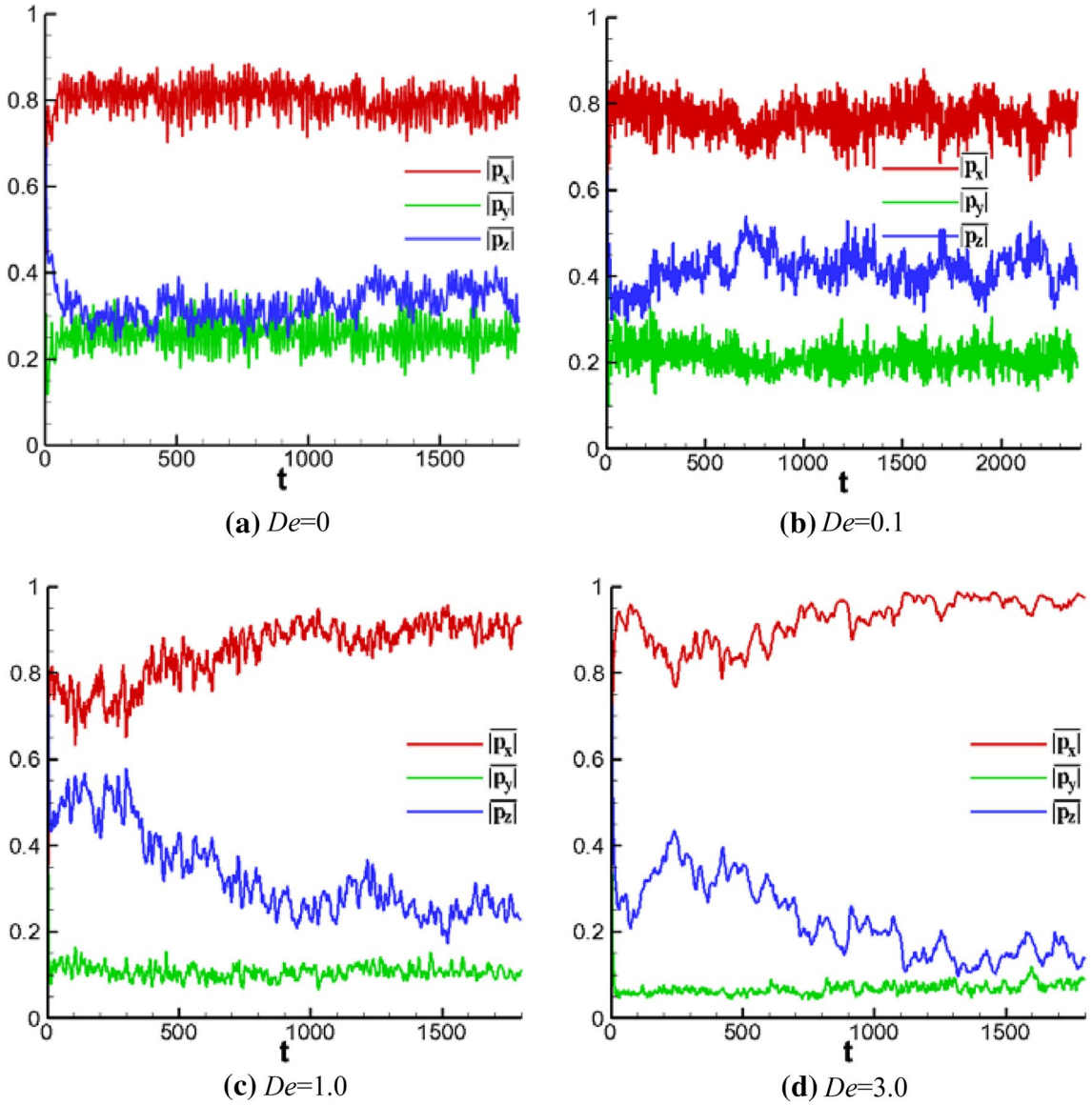

Fig. 9 The time developments of the average orientation components of 54 ellipsoids with random initial distributions and orientations for four Deborah numbers, **a** $De=0$, **b** $De=0.1$, **c** $De=1.0$, **d** $De=3.0$

The time developments of $\overline{|y_p|}$ at different Deborah numbers for 18 and 54 ellipsoids are shown in Fig. 7a, b, respectively. For the Newtonian fluid case, $\overline{|y_p|}$ do not change much with time for both N_p, while for the cases of viscoelastic fluids, the increases in $\overline{|y_p|}$ with time are clear, indicating the particle lateral migrations. Consistent with the single particle case, the increase of $\overline{|y_p|}$ with time is slow for $De=0.1$, and much faster for $De=1.0$, 3.0 and 4.0. For the same Deborah number, it takes more time for multiple ellipsoids to migrate to the walls than for a single ellipsoid. The increase rate of $\overline{|y_p|}$ for 54 ellipsoids is smaller than that for 18 ellipsoids, and the maximum value of $\overline{|y_p|}$ for 54 ellipsoids is also relatively smaller. This is because that almost all 18 ellipsoids can move into the particle layer adjacent to the wall with the thickness of one particle lateral size (Fig. 13), whereas for the case of $N_p=54$ multiple particle layers form near wall, as shown in Fig. 16.

The time development of $\overline{|p_x|}$, $\overline{|p_y|}$, $\overline{|p_z|}$ at different De for 18 and 54 ellipsoids are shown in Figs. 8 and 9, respectively. Fluctuations in the orientations can be seen in two figures. For $De=0.0$ and $De=0.1$, the rotational periods of

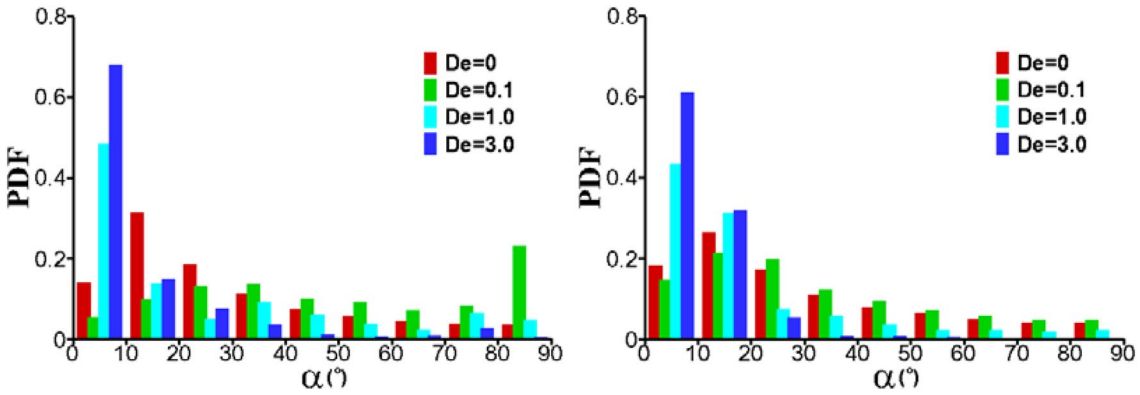

(a) N_p=18 **(b)** N_p =54

Fig. 10 The probability distribution function (PDF) of the angle between the ellipsoid major axis and the flow direction for four Deborah numbers and two particle numbers **a** $N_p = 18$, **b** $N_p = 54$, obtained from the last 50 simulation time units. The PDF is computed for the angle interval of every 10°

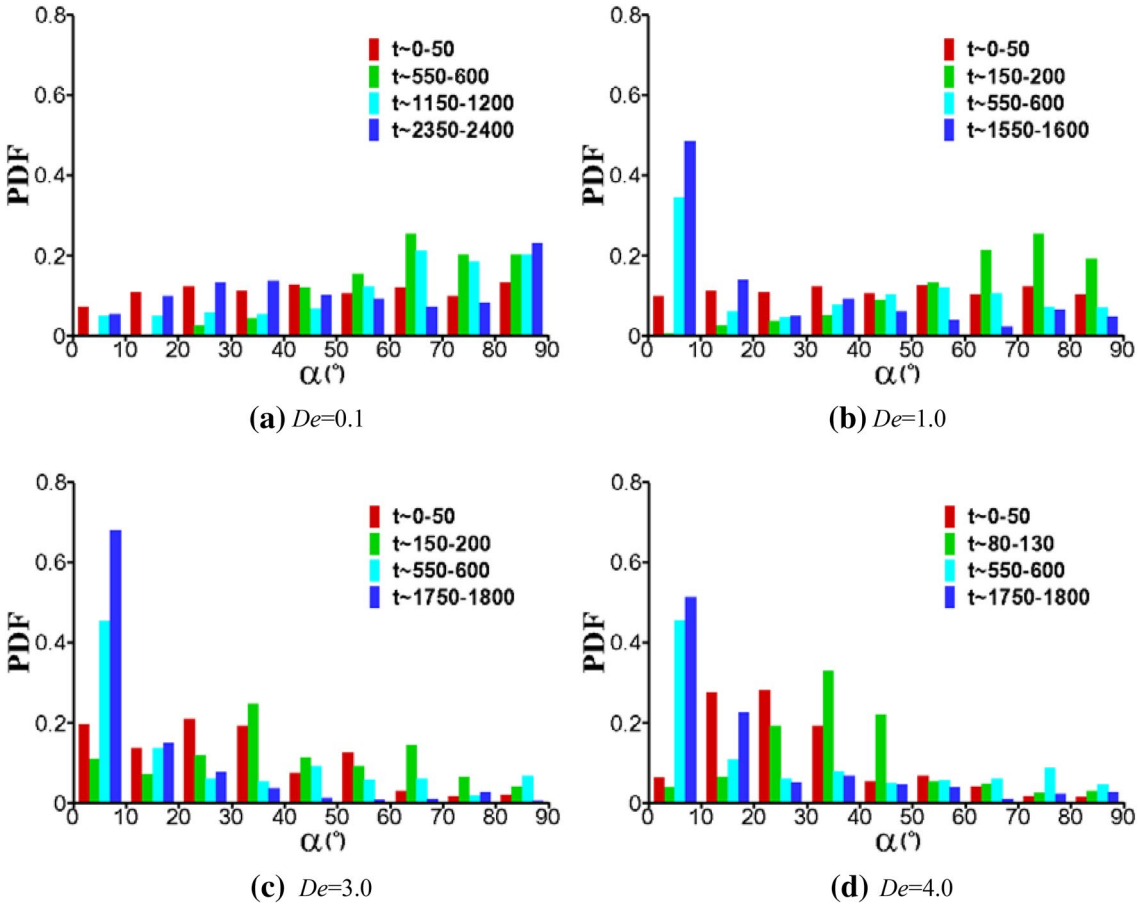

(a) *De*=0.1 **(b)** *De*=1.0

(c) *De*=3.0 **(d)** *De*=4.0

Fig. 11 The probability distribution function of the angle between the ellipsoids major axis and the flow direction in several time intervals for 18 ellipsoids at different Deborah numbers **a** $De = 0.1$, **b** $De = 1.0$, **c** $De = 3.0$, **d** $De = 4.0$

individual ellipsoids in shear flow are relatively small (Fig. 5a) so that the average orientations of the ellipsoids also fluctuate with high frequencies. For $De = 1.0$, the rotational periods of individual ellipsoids becomes relatively large (Fig. 5b), and for $De = 3.0$, there is no persistently periodic rotational motion (Fig. 5c), therefore, the average

orientations of the ellipsoids fluctuate with relatively low frequencies for $De = 1.0$ and 3.0. Even for the periodic rotation at low Deborah numbers, the particle major axis stays much longer when it moves through the flow-vorticity plane than through the shear-vorticity plane, thus $|p_y|$ are always small for all case and all times except the initial time in Figs. 8 and 9. For both $N_p = 18$ and 54 at $De = 0.0$, $|p_x|$ increase at the initial time stage and then fluctuate around the average value of around 0.8. This flow alignment is expected to be mainly resulted from the particle interactions. For the viscoelastic fluid cases at $De = 0.1$, 1.0 and 3.0 and $N_p = 18$, $|p_z|$ increase and $|p_x|$ decrease at initial stages. This can be explained by the earlier observation that a single ellipsoid undergoing lateral migration turns toward the vorticity direction (Figs. 5 and 6). Note that for $De = 3.0$, the increase in $|p_x|$ can be seen at very early time before it drops in Fig. 8d, which is probably caused by the initial turning of ellipsoids toward the flow-vorticity plane; the turning time is larger for a higher De. With more particles migrating to the wall region, $|p_z|$ begin to decrease and $|p_x|$ increase, which indicates that the particle interactions and the wall effect render the particles to align with the flow direction. The terminal average orientation is closer to the flow direction for a higher Deborah number. The results for $N_p = 54$ are similar, however, the enhanced effect of the particle interactions leads to weaker turning of the particles toward the vorticity direction at the initial stage and stronger alignment in the flow direction for most times.

The wall confinement can directly affect the particle orientation, and on the other hand can affect the orientation indirectly via the particle interactions. As more particles migrate to the wall region, the particle volume fraction in the wall region increases, which makes the particles more strongly aligned in the flow direction. A single migrating ellipsoid tends to align itself with the vorticity direction (Figs. 5 and 6). It can be observed that for the multiple-particle case, the isolated ellipsoids are often aligned in the vorticity direction (see Figs. 12 and 13), like the single particle case. At the initial stage, the particles are distributed in the space almost homogeneously, and thus the possibility of the occurrence of isolated particles is higher, resulting in the shift of the average orientation toward the vorticity direction. With more particles migrating to the wall region, the possibility of the occurrence of isolated particles becomes lower, which could be partly responsible for the shift of the average orientation toward the flow direction.

The probability density functions (PDF) of the angle between the ellipsoid major axis and the flow direction, α, computed from the last 50 time units for $N_p = 18$ and $N_p = 54$, are plotted in Fig. 10a, b, respectively. The angle is defined in the range of $0 \le \alpha \le 90°$, and the PDF is computed for nine intervals of each 10°. For the Newtonian

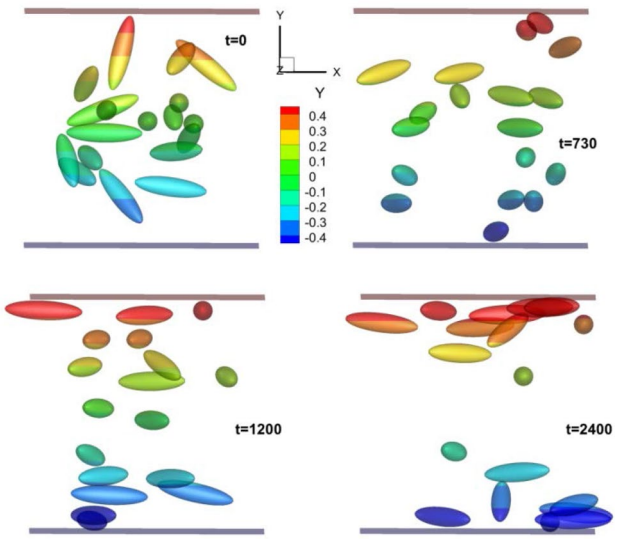

Fig. 12 Snapshots of the ellipsoids at different times for $N_p = 18$, $De = 0.1$ (view in the vorticity direction). The color represents the y-position (color figure online)

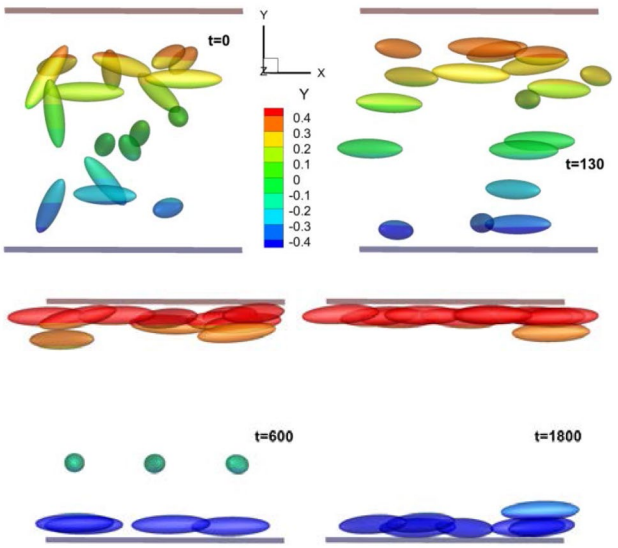

Fig. 13 Snapshots of the ellipsoids at different times for $N_p = 18$ and $De = 4.0$ (view in the vorticity direction). The color represents the y-position (color figure online)

fluid, the PDF of α is largest in the interval of 10°–20° and the particle number does not have a significant effect on the probability distribution. For $De = 0.1$, the PDF of α is largest in 80°–90° for the case of $N_p = 18$, but has relatively large values in 0°–30° for $N_p = 54$, indicating that the particle interactions can lead to the change of the preferential orientation from the spanwise direction to the flow direction. For $De = 1.0$ and 3.0, the probabilities of α near the flow direction ($0 \le \alpha \le 20°$) are large, which

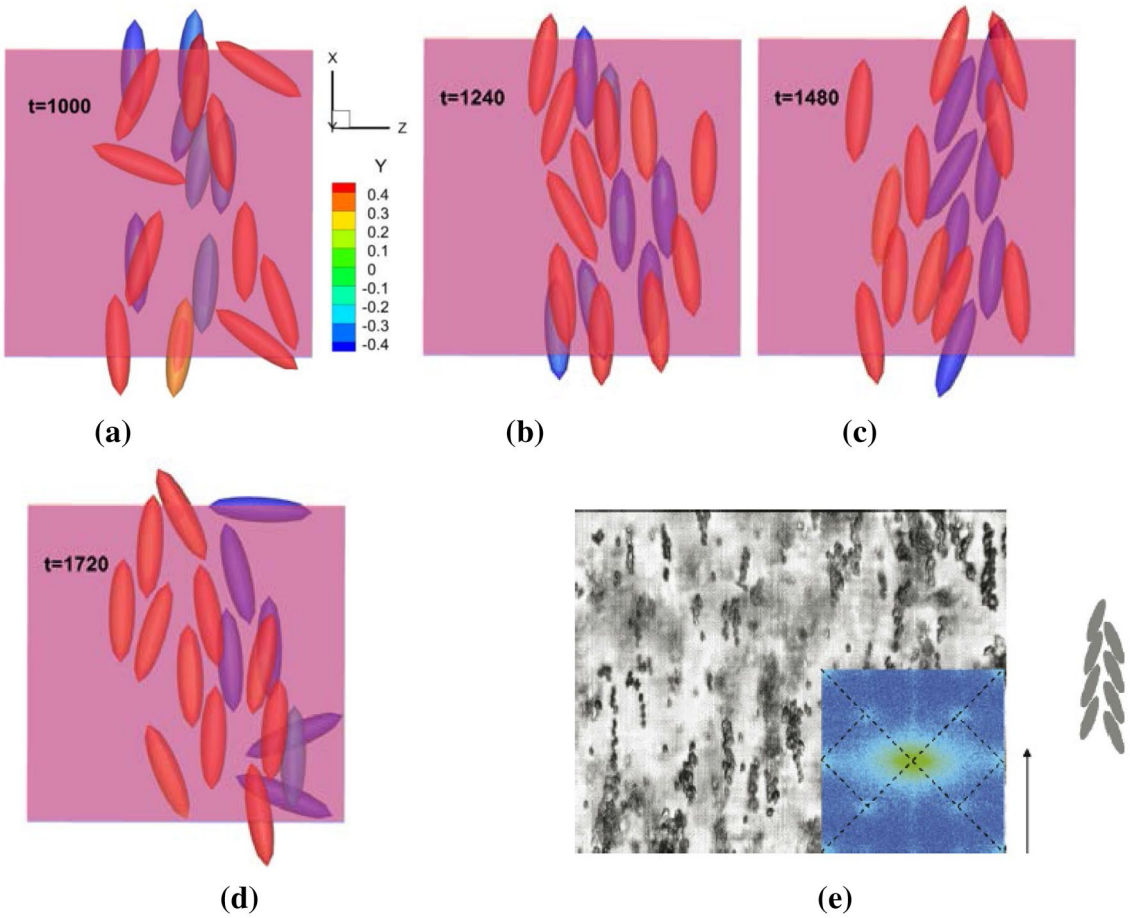

Fig. 14 Snapshots of the ellipsoids at different times for $N_p = 18$ and $De = 4.0$ in our simulations (**a**–**d**), and of the experiments of Gunes et al. (2008) for a highly viscoelastic fluid (**e**) (view in the shear direction). Figure **e** is taken from Gunes et al. (2008) with permission

means the flow alignment. The flow alignment at $De = 3.0$ is stronger than at $De = 1.0$.

The PDFs of the angle between the ellipsoids major axis and the flow direction for several time intervals and 18 ellipsoids at different Deborah numbers are shown in Fig. 11. Figure 8 shows that $\overline{|p_z|}$ increase and $\overline{|p_x|}$ decrease at initial stages for $De = 0.1$, 1.0 and 3.0, which can be explained by the turning of the isolated ellipsoids toward the vorticity direction. From Fig. 11, in the second stage (the green bars, $t = 550$–600 for $De = 0.1$ and t is around 150 for other De), the increase in $\overline{|p_z|}$ is mainly caused by the increase in large α of 60°–90° for $De = 0.1$ and 1.0, in both intermediate α of 30°–50° and large α of 60°–90° for $De = 3.0$, and in intermediate α of 30°–50° for $De = 4.0$, as compared to the first stage of $t = 0$–50 (the red bars in Fig. 11). In the third stage for $De = 1.0$, 3.0 and 4.0 ($t = 550$–600), the PDFs of small α of 0°–10° become large, as most particles migrate to the wall region (Fig. 13) and many particles are aligned along the flow direction due to the wall effect and the particle interactions. The flow alignment is further enhanced in the fourth stage when the particles are closer to the wall.

The snapshots of the ellipsoids at several times are shown in Fig. 12 for $N_p = 18$ and $De = 0.1$, in Figs. 13 and 14 for $N_p = 18$ and $De = 4.0$, Fig. 15 for $N_p = 54$ and $De = 0.1$, and Figs. 16 and 17 for $N_p = 54$ and $De = 4.0$. Figure 12 shows that for $N_p = 18$ and $De = 0.1$, the ellipsoids tend to turn the major axes from the initial random orientations toward the vorticity direction, and the particles near the wall in cluster tend to turn toward the flow direction. Figure 13 shows more clearly that the isolated particles are more likely to align in the vorticity direction, whereas the aggregated particles near the wall are more likely to align in the flow direction, for $N_p = 18$ and $De = 4.0$.

The snapshots from the view of the shear direction in Figs. 14 and 17 show the spanwise aggregation of the particles. The end-to-end aggregation of the particles (i.e., particle chain) is not observed, unlike the spherical particles. The aligning structure with two slightly tilted ellipsoids aggregated in the spanwise direction, as shown in Fig. 14,

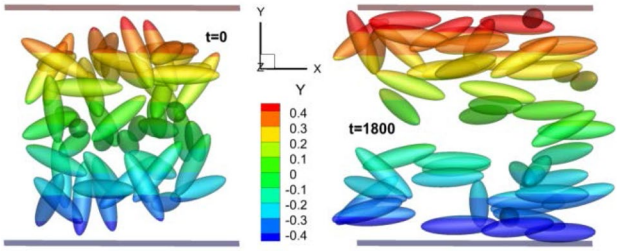

Fig. 15 Snapshots of the ellipsoids at different times for $N_p = 54$ and $De = 0.1$ (view in the vorticity direction). The color represents the y-position (color figure online)

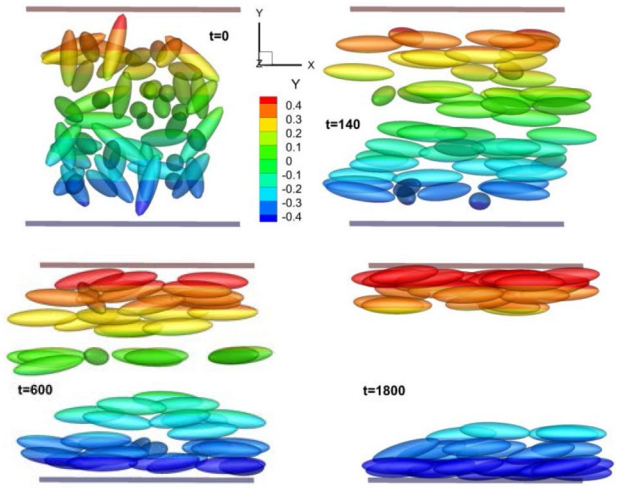

Fig. 16 Snapshots of the ellipsoids at different times for $N_p = 54$ and $De = 4.0$ (view in the vorticity direction). The color represents the y-position (color figure online)

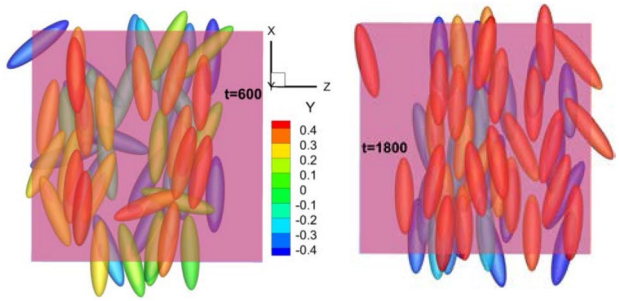

Fig. 17 Snapshots of the ellipsoids at different times for $N_p = 54$ and $De = 4.0$ (view in the shear direction). The color represents the y-position (color figure online)

can exist for a relatively long time. Such structure is similar to that observed in the experiment of Gunes et al. (2008), as shown in Fig. 14e.

The distributions of the particle volume fractions of 54 ellipsoids along the shear direction at different times for $De = 0.1$ and $De = 4.0$ are given in Fig. 18, which shows the slow migration of the ellipsoids at $De = 0.1$ and the fast migration at $De = 4.0$. For $t > 1000$ and $De = 4.0$, two peaks in the particle volume fraction near each wall can be observed in Fig. 18b, corresponding to two particle layers forming near each wall, as shown in Fig. 16.

Only one aspect ratio of 4 is studied. A more slender particle has a larger rotational period and stays longer when its orientation is turning close to the flow direction. It was shown that the transition from the log-rolling mode to the flow alignment occurred at a smaller Deborah number for a more slender particle (D'Avino et al. 2014). Therefore, stronger flow alignment is expected for more slender particles at the same Deborah number.

4 Conclusions

The motion of neutrally buoyant ellipsoids with a blockage ratio of $\beta = 1/3$ and an aspect ratio of $A_r = 4$ in a planar Couette flow of a Giesekus viscoelastic fluid with negligibly small inertial effects has been simulated with a fictitious domain method. From our results, the following conclusions can be drawn:

1. For a single ellipsoid initially placed in the mid-plane between the two plates, the ellipsoid major axis rotates around the vorticity axis in a kayaking mode at relatively low Deborah numbers, and is tilted in the flow-vorticity plane when the Deborah number exceeds a critical value, with the orientation being closer to the flow direction for a larger De.
2. For a single ellipsoid initially not placed in the mid-plane, the ellipsoid undergoes lateral migration toward the nearby wall, and turns its orientation to the vorticity axis (log-rolling) at relatively low Deborah numbers and to a direction close to the vorticity axis at large Deborah numbers, unlike the ellipsoid placed in the mid-plane without lateral migration.
3. For the multiple-ellipsoid case, there exists a transient stage where the average orientation of the ellipsoids turns toward the vorticity axis for all nonzero Deborah numbers studied. The isolated ellipsoids are more likely to align with the vorticity direction even for $De = 4$, and both the particle interactions and the wall effect drive the ellipsoids to align with the flow direction. Particle aggregation and the dynamic aligning structures are observed at large Deborah numbers.

Limited by our computer resources, only a small Couette cell is considered. The interactions of the multiple particles

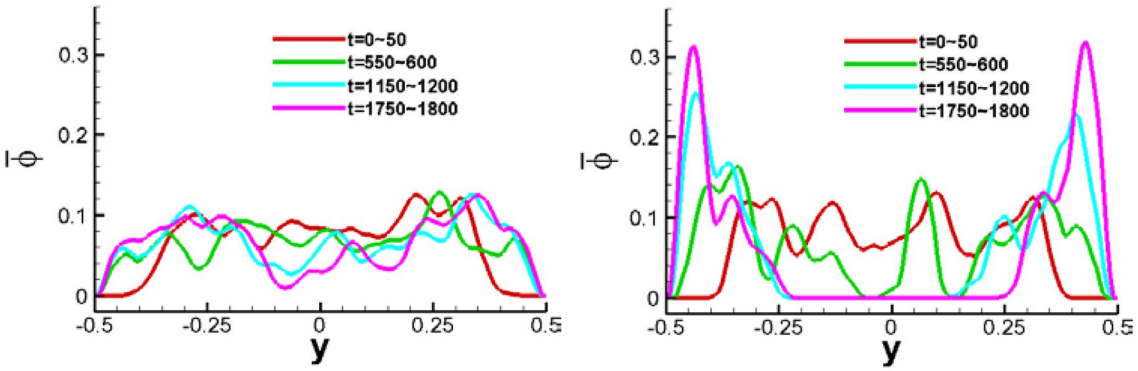

Fig. 18 The distributions of the particle volume fraction at different times for $N_p = 54$ and **a** $De = 0.1$, **b** $De = 4.0$

in a large system and the motion of the ellipsoids in the Oldroyd-B fluid may be worthy of further study.

Acknowledgements The work was supported by the National Natural Science Foundation of China (Grant Nos. 11632016, 91752117).

References

Bartram E, Goldsmith HL, Mason SG (1975) Particle motions in non-Newtonian media, III. Further observations in viscoelastic fluids. Rheol Acta 14:776–782

Borzacchiello D et al (2016) Orientation kinematics of short fibres in a second-order viscoelastic fluid. Rheol Acta 55:397–409

Brunn P (1980) The motion of rigid particles in viscoelastic fluids. J Non-Newton Fluid Mech 7:271–288

Caserta S, D'Avino G, Greco F, Guido S, Maffettone PL (2010) Migration of a sphere in a viscoelastic fluid under planar shear flow: experiments and numerical predictions. Soft Matter 7:1100–1106

Cohen C, Chung B, Stasiak W (1987) Orientation and rheology of rod-like particles with weak Brownian diffusion in a 2nd-order fluid under simple shear-flow. Rheol Acta 26:217–232

Crowe CT et al (2011) Multiphase flows with droplets and particles. CRC Press, Boca Raton, FL

D'Avino G, Maffettone PL (2015) Particle dynamics in viscoelastic liquids. J Non-Newton Fluid Mech 215:80–104

D'Avino G, Tuccillo T, Hulsen MA, Greco F, Maffettone PL (2010a) Numerical simulations of particle migration in a viscoelastic fluid subjected to shear flow. Comput Fluids 39:709–721

D'Avino G, Maffettone PL, Greco F, Hulsen MA (2010b) Viscoelasticity-induced migration of a rigid sphere in confined shear flow. J Non-Newton Fluid Mech 165:466–474

D'Avino G, Hulsen MA, Greco F, Maffettone PL (2014) Bistability and metabistability scenario in the dynamics of an ellipsoidal particle in a sheared viscoelastic fluid. Phys Rev E 89:043006

D'Avino G, Greco F, Maffettone PL (2015) Rheology of a dilute viscoelastic suspension of spheroids in unconfined shear flow. Rheol Acta 54:915–928

D'Avino G, Greco F, Maffettone PL (2017) Particle migration due to viscoelasticity of the suspending liquid and its relevance in microfluidic devices. Annu Rev Fluid Mech 49:341–360

D'Avino G, Hulsen MA, Greco F, Maffettone PL (2019) Numerical simulations on the dynamics of a spheroid in a viscoelastic liquid in a wide-slit microchannel. J Non-Newton Fluid Mech 263:33–41

de Oliveira IS, den Otter WK, Briels WJ (2013) Alignment and segregation of bidisperse colloids in a shear-thinning viscoelastic fluid under shear flow. Europhys Lett 101:28002

Férec J, Bertevas E, Khoo BC, Ausias G, Thien NP (2017) Steady-shear rheological properties for suspensions of axisymmetric particles in second-order fluids. J Non-Newton Fluid Mech 239:62–72

Gauthier F, Goldsmith HL, Mason SG (1971) Particle motions in non-Newtonian media. I. Couette flow. Rheol Acta 10:344–364

Glowinski R, Pan TW, Hesla TI, Joseph DD (1999) A distributed lagrange multiplier/fictitious domain method for particulate flows. Int J Multiph Flow 25:755–794

Gunes DZ, Scirocco R, Mewis J, Vermant J (2008) Flow-induced orientation of nonspherical particles: effect of aspect ratio and medium rheology. J Non-Newton Fluid Mech 155:39–50

Harlen OG, Koch DL (1993) Simple shear-flow of a suspension of fibers in a dilute polymer-solution at high Deborah number. J Fluid Mech 252:187–207

Hobbie EK et al (2003) Orientation of carbon nanotubes in a sheared polymer melt. Phys Fluids 15:1196–1202

Huang H, Lu X (2017) An ellipsoidal particle in tube Poiseuille flow. J Fluid Mech 822:664–688

Huang PY, Feng J, Hu HH, Joseph DD (1997) Direct simulation of the motion of solid particles in Couette and Poiseuille flows of viscoelastic fluids. J Fluid Mech 343:73–94

Huang H, Yang X, Krafczyk M, Lu X (2012) Rotation of spheroidal particles in Couette flows. J Fluid Mech 692:369–394

Iso Y, Koch DL, Cohen C (1996a) Orientation in simple shear flow of semi-dilute fiber suspensions 1. Weakly elastic fluids. J Non-Newton Fluid Mech 62:115–134

Iso Y, Koch DL, Cohen C (1996b) Orientation in simple shear flow of semi-dilute fiber suspensions 2. Highly elastic fluids. J Non-Newton Fluid Mech 62:135–153

Jaensson NO, Hulsen MA, Anderson PD (2016) Direct numerical simulation of particle alignment in viscoelastic fluids. J Non-Newton Fluid Mech 235:125–142

Jeffery GB (1922) The motion of ellipsoidal particles immersed in a viscous fluid. Proc R Soc Ser A 102:161–179

Johnson SJ, Salem AJ, Fuller GG (1990) Dynamics of colloidal particles in sheared non-newtonian fluids. J Non-Newton Fluid Mech 34:89–121

Karnis A, Gldsmith HL, Masion SG (1966) The flow of suspensions through tubes. Part V: inertial effects. Can J Chem Eng 44:181–193

Leal LG (1975) Slow motion of slender rod-like particles in 2nd order fluid. J Fluid Mech 69:305–337

Leer BV (1979) Towards the ultimate conservative difference scheme. V. A second-order sequel to Godunov's method. J Comput Phys 32:101–136

Lin A, Han SP (2002) On the distance between two ellipsoids. SIAM J Optim 13:298–308

Lin J, Wang Y, Zhang P, Ku X (2018) Mixing and orientation behaviors of cylindrical particles in a mixing layer of an Oldroyd-B fluid. Chem Eng Sci 176:270–284

Lu X, Liu C, Hu G, Xuan X (2017) Particle manipulations in non-newtonian microfluidics: a review. J Colloid Interface Sci 500:182–201

Lyon MK, Mead DW, Elliott RE, Leal LG (2001) Structure formation in moderately concentrated viscoelastic suspensions in simple shear flow. J Rheol 45:881–890

Madani A et al (2010) Fractionation of non-Brownian rod-like particle suspensions in a viscoplastic fluid. Chem Eng Sci 65:1762–1772

Michele J, Patzold R, Donis R (1977) Alignment and aggregation effects in suspensions of spheres in non-Newtonian media. Rheol Acta 16:317–321

Pan TW, Chang CC, Glowinski R (2008) On the motion of a neutrally buoyant ellipsoid in a three-dimensional Poiseuille flow. Comput Methods Appl Mech Eng 197:2198–2209

Pasquino R, Snijkers F, Grizzuti N, Vermant J (2010) The effect of particle size and migration on the formation of flow-induced structures in viscoelastic suspensions. Rheol Acta 49:993–1001

Pasquino R, Panariello D, Grizzuti N (2013) Migration and alignment of spherical particles in sheared viscoelastic suspensions: a quantitative determination of the flow-induced self-assembly kinetics. J Colloid Interface Sci 394:49–54

Pasquino R, D'Avino G, Maffettone PL, Greco F, Grizzuti N (2014) Migration and chaining of noncolloidal spheres suspended in a sheared viscoelastic medium: experiments and numerical simulations. J Non-Newton Fluid Mech 203:1–8

Qi DW, Luo LS (2003) Rotational and orientational behaviour of three-dimensional spheroidal particles in Couette flows. J Fluid Mech 477:201–213

Rosén T, Do-Quang M, Aidun CK, Lundell F (2015) The dynamical states of a prolate spheroidal particle suspended in shear flow as a consequence of particle and fluid inertia. J Fluid Mech 771:115–158

Saffman PG (1956) On the motion of small spheroidal particles in a viscous liquid. J Fluid Mech 1:540–553

Scirocco R, Vermant J, Mewis J (2004) Effect of the viscoelasticity of the suspending fluid on structure formation in suspensions. J Non-Newton Fluid Mech 117:183–192

Trofa M, D'Avino G, Hulsen MA, Greco F, Maffettone PL (2016a) Numerical simulations of the dynamics of a slippery particle in Newtonian and viscoelastic fluids subjected to shear and poiseuille flows. J Non-Newton Fluid Mech 228:46–54

Trofa M, D'Avino G, Hulsen MA, Maffettone PL (2016b) The effect of wall slip on the dynamics of a spherical particle in Newtonian and viscoelastic fluids subjected to shear and poiseuille flows. J Non-Newton Fluid Mech 236:123–131

Wang P, Yu Z, Lin J (2018) Numerical simulations of particle migration in rectangular channel flow of Giesekus viscoelastic fluids. J Non-Newton Fluid Mech 262:142–168

Won D, Kim C (2004) Alignment and aggregation of spherical particles in viscoelastic fluid under shear flow. J Non-Newton Fluid Mech 117:141–146

Yu Z, Shao X (2007) A direct-forcing fictitious domain method for particulate flows. J Comput Phys 227:292–314

Yu Z, Wachs A (2007) A fictitious domain method for dynamic simulation of particle sedimentation in Bingham fluids. J Non-Newton Fluid Mech 145:78–91

Yu Z, Phan-Thien N, Fan Y, Tanner R (2002) Viscoelastic mobility problem of a system of particles. J Non-Newton Fluid Mech 104:87–124

Yu Z, Wachs A, Peysson Y (2006) Numerical simulation of particle sedimentation in shear-thinning fluids with a fictitious domain method. J Non-Newton Fluid Mech 136:126–139

Yu Z, Phan TN, Roger IT (2007) Rotation of a spheroid in a Couette flow at moderate Reynolds numbers. Phys Rev E 76:026310